Tuning the Indirect Band Gap of Square Metallic Superlattices

M. A. Kher-Elden[a]*, Z. M. Abd El-Fattah[b], O. Yassin[c], M. M. El-Okr[d]

[a,b,c,d]*Physics Department, Faculty of Science, Al-Azhar University, Nasr City, E-11884, Cairo, Egypt*

[a]*Email: mohammad.khereldeen@gmail.com*

Abstract

Shockley surface states at noble metal surface are textbook examples of "*free-electron*" dispersions in solids. Their interaction with lateral periodic arrays of defects drastically modifies this simple band structure picture at different rates. Here, the plane wave expansion method has been used to investigate the modification of the band structure of metal surfaces in the present of two-dimensional square array of scatterers. Such nanopatterned square superlattices were found to trigger the opening of an indirect band gap at the boundaries of the superlattice Brillouin zone. Additionally, both the momentum-position and the size of these gaps could be tuned by varying the superlattice periodicity and the scattering potential, respectively. These findings provide a route towards engineering the electronic structure of patterned metal surfaces.

Keywords: Plane wave expansion; metallic superlattices; band structure; Shockley surface stats.

1. Introduction

Two-dimensional nanostructures made of inorganic and organic networks on metallic substrates have received much attention in recent years [1]. Such self-assembled nanopatterned surfaces found promising applications in all fields of nanoscience, particularly nanoelectronics [2], chemical sensing [3], and as template surfaces for selective molecular assembly [4,5]. Their fabrication has progressed rapidly such that patterns with complex unit cells and almost of any arbitrary geometry could be fabricated [6].

----

* Corresponding author.

The use of pre-patterned surfaces to guide adsorption processes [7] has been demonstrated on a variety of spontaneously nanostructured substrates such as dislocation networks [8], vicinal surfaces [9], and self-ordered biphase systems [10,11]. With these, the delicate balance between adsorbate-adsorbate and adsorbate-substrate interactions [12] could be finely tuned to achieve the desired molecular or metallic assembly on crystal surfaces. At the surface of the (111)-oriented noble metal substrates electrons exhibiting free-electron parabolic dispersion with distinct dispersion parameters for each noble metal surface are reported [13,14]. Such dispersion parameters have been measured by angle-resolved photoemission spectroscopy (ARPES) for the three *"flat"* (111) noble metal surfaces [15]. The interaction of the free electrons with 2D periodic arrays of scatterers modifies these Shockley dispersions at different rates. This has been reported for 1D array of steps, e.g., in vicinal surfaces [16], and for 2D hexagonal and honeycomb arrays, e.g., 1 ML Ag/Cu(111) [17] and DPDI/Cu(111) [18], respectively. The overall effect of the scatterers is an upward energy shift and the opening of energy gaps at some high symmetry points. In these regards, the electronic structure of squarely patterned metal surfaces is rarely present in literature in spite the possible experimental realization. One such an experimental example of a 2D squarely nanopatterned metal surface is the N/Cu(001) [19]. A two-dimensional square lattice of nitrogen-adsorbed areas with a typical lateral dimension of roughly 5 nm appeared when the average density of adsorbed nitrogen atoms on Cu(001) was 35% of that of the surface Cu atoms.

To this end, the article presents systematic and detailed theoretical study of electron scattering problem in 2D square superlattices, formed on metal surfaces, using electron plane wave expansion method (EPWE). By systematic variation in the scattering parameters (i.e., the periodic potential and periodicity), the effect of both on the electronic structure was obtained by the detailed analysis of series of the full band structures, constant energy surfaces (CES), and local density of states (LDOS). Specifically, such square superlattices predominantly exhibit an indirect band gap which could be largely tuned through controlling the scatterer's parameters.

2. Computational method

The electron plane wave expansion method (EPWE) has been used throughout the present study. Within this methodology, Schrödinger equation for electrons encountering a square periodic array of circular scatterers, each encloses an effective potential V, is written as:

$$\left(-\frac{\nabla^2}{2} + V_s(r) - E_{nk}\right)\psi_{nk} = 0 \tag{1}$$

where $k^2 = 2m_{eff} E/\hbar^2$ is the electron momentum, E is the electron energy, and m_{eff} is the electron effective mass. Both the wavefuction and the periodic potential are expanded in the form of Fourier expansions, in order to obtain the following central equation after substitution in equation (1) [20],

$$\sum_{G''}\left[\left(\frac{|k+G|^2}{2} - E_{nk}\right)\delta(G - G'') + V_{G-G''}\right]c_{G''}(k) = 0 \tag{2}$$

where $c_{G''}$ and $V_{G-G''}$ are the Fourier coefficients of the wavefunction and potential, respectively, and G, G'' are

two reciprocal lattice vectors, while the delta function $\delta(G - G'')$ ensures that first term in the sum over G'' is zero unless $G'' = G$.

Equation (2) is then solved numerically by terminating the expansion at some finite reciprocal lattice vectors ($G'' = G^{max}$). In the present work a decent convergence is achieved for $G^{max} \geq 5$.

3. Results and discussions

3.1. Electronic Structure
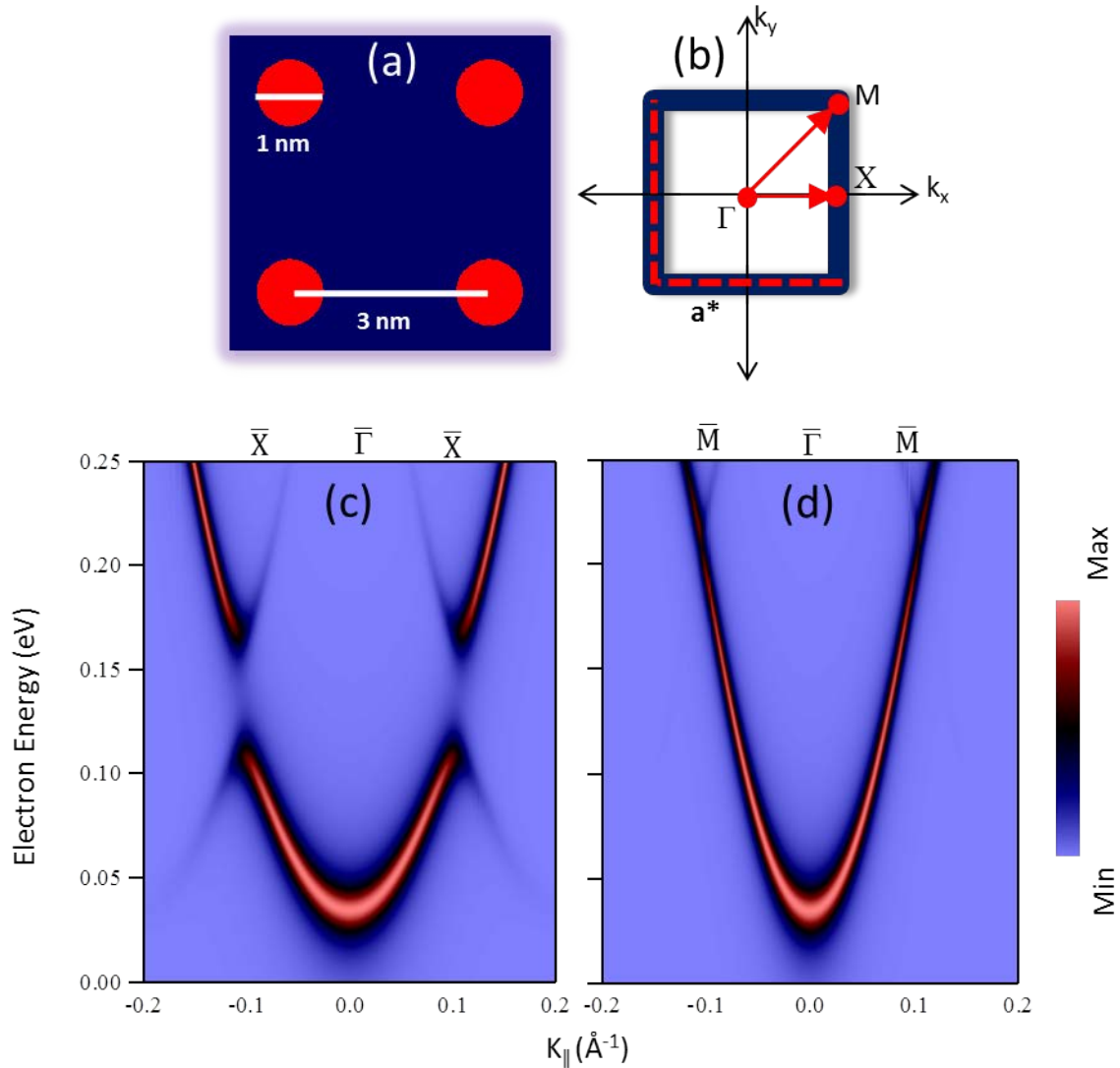
Figure 1: (a) The geometry used in EPWE calculations. The blue area defines a metal surface and the red circles represent square array of defects. (b) The Brillouin zone of the geometry defined in (a). (c,d) The EPWE simulated photoemission intensity showing the band dispersion for the patterned metal surface along $\overline{\Gamma X}$ (c) and $\overline{\Gamma M}$ (d) directions.

Figure 1(a) presents the surface potential landscape used as input for EPWE. It simply, describes metal surface (blue) with a periodic array of circular (red) scatterers. Given the known parabolic dispersion for flat metal surfaces, the potential within the blue region is set to constant ($V_0 = 0$), while the potential barrier inside the circular bases has height of $V_1 = 700$ meV. This choice of the scattering potential is intended to be within the same order of magnitude for reported studies. Both the circle diameter and superlattice constant were set to 1 nm and 3 nm respectively, whereas the effective mass used was 0.42 m_e, i.e., practically the same as reported experimentally for Ag(111) and Cu(111) [21]. The simulated photoemission intensity for the system presented in (a) is displayed in Fig. 1(c,d). The calculations are performed along both $\overline{\Gamma X}$ and $\overline{\Gamma M}$ directions (red arrows) of the first BZ (blue square in Fig. 1(b)). One clearly sees in (c) a parabolic dispersion with a band gap opening at the BZ boundary (i.e., the $\overline{X}$-point) together with a rigid upward shift (~ 35 meV) for the surface state band minimum at $\overline{\Gamma}$-point. On other hand, the band dispersion in (d) also exhibits a weak band gap opening at the BZ corner (i.e., the $\overline{M}$-point). The $\overline{X}$-point and $\overline{M}$-point gaps size amount to ~ 60 meV and ~ 15 meV, respectively. Additionally, the energetic positions of these gaps are clearly different, indicating an indirect character of the full $\overline{\Gamma X M \Gamma}$ gap. In order to elucidate more details of the square nanopatterned surface, the electronic band structure along the ($\overline{\Gamma X M \Gamma}$) direction and the constant energy surfaces (CES) are calculated and presented in Fig. 2. In (a) the band structure calculation confirms the indirect semiconducting band gap of this surface state. The minimum of the conduction band (red line) does not occur at the same k value as the valence band maximum (green line). To trace these electronic details at all k points inside the BZ the CES were calculated by EPWE at different set of fixed energies. Figure 2(b-e) depicts the simulated CESs taken at the black dashed lines in (a), i.e., at 110 meV, 130 meV, 170 meV, and 210 meV, respectively. The white dashed square in each CES map define the borders of the first BZ. The first CES in (b) taken at electron energy of $E = 110$ meV, i.e., barely at the lower edge of the $\overline{X}$-point gap, exhibits intensity reduction only at the four equivalent $\overline{X}$-points, confirming the beginning of energy gaps at these points. At electron energies within this gap, e.g., $E = 130$ meV, the intensity reduction was enhanced for all k-points on the surface BZ, except in the vicinity of the corners defining the $\overline{M}$-points, Fig. 2(c). Furthermore, these CES exhibit a significant deviation from the "circular" contours of free electrons, where the CES clearly contain "flat" segments. The length of these segments is reduced at the expense of the intensity depletion regions for increased electron energies within the gap. Exactly at the conduction band minimum, i.e., $E = 170$ meV, the simulated CES is presented in (d). Four electron pockets showed up at the equivalents $\overline{X}$-gaps. The last CES in (e) is taken approximately at the center of the $\overline{M}$-gap i.e., at electron energy of $E = 210$ meV. The relatively low intensity at the BZ corners corresponds to the four weak gaps at these particular momentum positions. The correspondence between electronic structure in real and reciprocal space is experimentally brought by scanning tunneling spectroscopy (STS). This is an experimental technique that probes the local density of electronic states (LDOS), which in turns contains information on the band gap of nanostructured surfaces and local electronic behavior at the atomic scale [22]. Using EPWE, the LDOS are calculated at three different cites, i.e., specific points in the real space geometry in Fig. 3(a). These points were chosen as variations in the LDOS are expected to be significant according to symmetry considerations. The LDOS at the center of the circular potential barriers (black) is very low at all energies compared to the other two points (blue and red). This confirms that electrons are possibly excluded from regions with relatively large potential values. Likewise, the LDOS taken at the center of the unit cell (red), and the center of the side length (blue) where the potential is zero, are significantly higher and exhibit strong variations

with the electron energy. The inflection points (vertical green line) at ~ 35 meV for all spectra define the $\bar{\Gamma}$-point energy, in agreement with band structure calculations. The blue and red LDOS, in addition, exhibit maxima and minima which indicate the presence of $\bar{X}$-point and $\bar{M}$-point gaps, where the vertical dashed lines define the valence (conduction) band maximum (minimum).
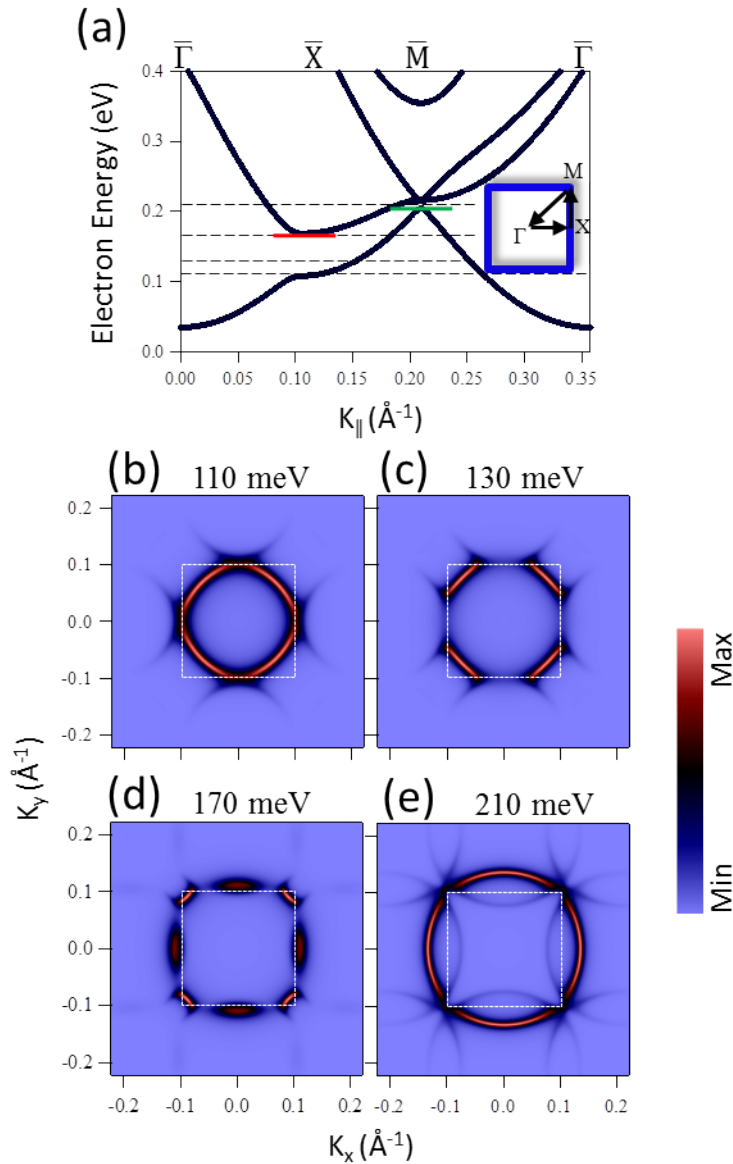
Figure 2: (a) Calculated band structure using EPWE along the $\overline{\Gamma XM\Gamma}$ direction, i.e, along the black arrows of the first Brillouin zone (blue square). (b-e) Simulated constant energy surfaces taken at the black dashed lines in (a), i.e., at 110, 130, 170, and 210 meV respectively.

In order to gain information on the LDOS at all real-space lattice points, 2D-LDOS calculations were performed at the three electron energies indicated by the black dashed lines in (a), i.e., at 105 meV (b), 170 meV (c), and 210 meV (d). The blue, red, and black points are overlaid for direct comparison with Fig. 3(a). The LDOS has a minimum intensity value at all, and nearby, the black points, i.e., at the bases, at all energies. However, the

LDOS values at the red and blue points follow some intensity modulation in accordance with symmetry considerations [23]. In particular, the reduction of LDOS intensity at the red point directly mimic the influence of the energy gaps, as shown in (b,c,d).
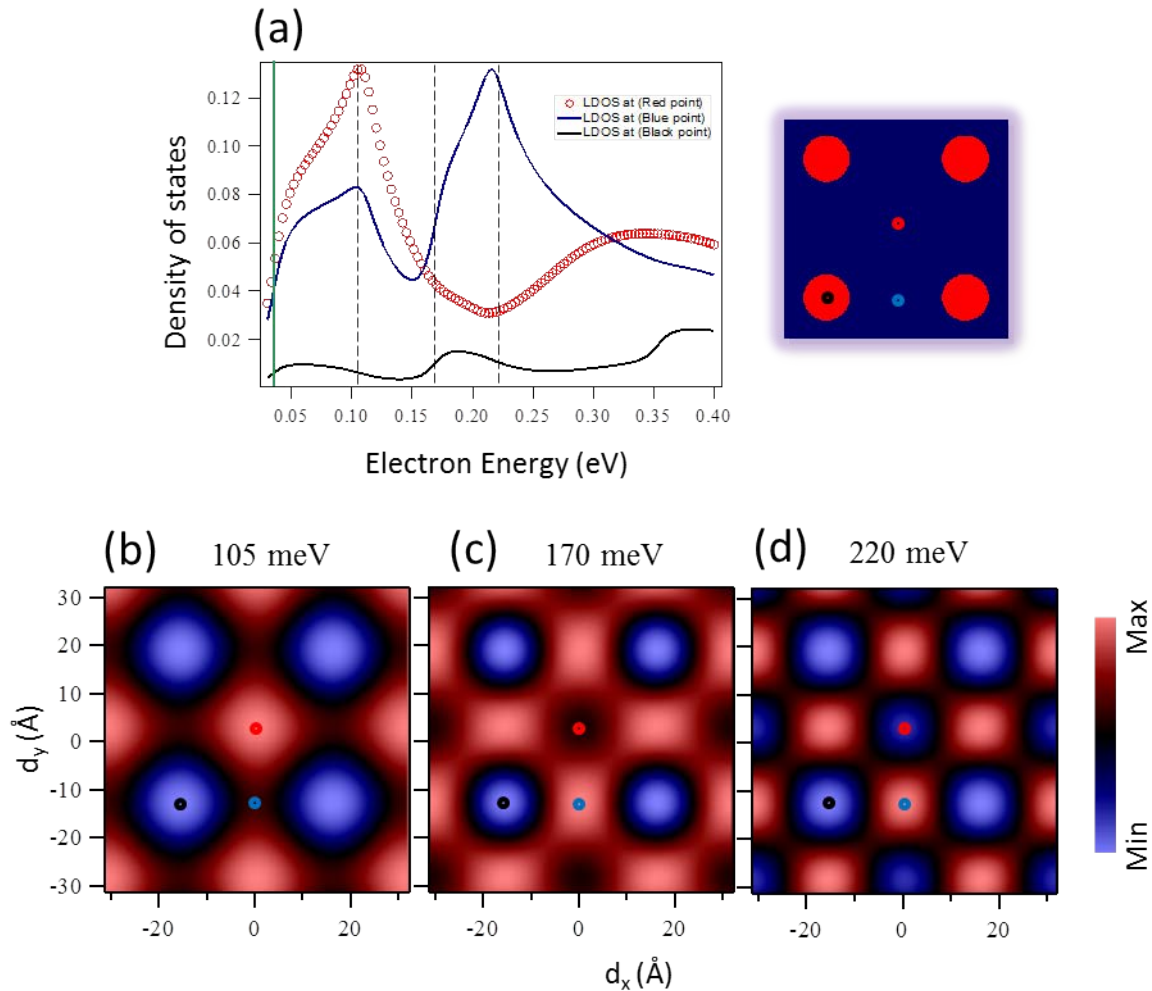

Figure 3: (a) The energy-dependent local density of states (LDOS) calculated by the EPWE for three real space points. (b-d) The 2D-LDOS taken at three electron energies.

3.2. Effect of periodic potential

With the previous analysis, the surface state at metal surface interacting with square array of defects exhibits band gap openings at the symmetry points and LDOS modulations due to these gaps and the symmetry of the structure. In the following, the effect of the scattering potential on the electronic structure of squarely patterned metal surface shall be discussed. Figure 4 displays the electronic band structure as calculated by EPWE along the ($\overline{\Gamma X M \Gamma}$) directions (a). All other geometrical and physical parameters in these calculations were identical to those previously discussed except for the height of the potential barrier (V_1), which is changed from 700 meV to 4.7 eV. The surface state exhibits a parabolic dispersion with much wider gaps at the $\overline{X}$ and $\overline{M}$ points, together with a larger rigid upward shift for the band minimum at $\overline{\Gamma}$-point than the values of band structure depicted in

Fig. 2(a). The band dispersion has a valence band maximum (green line) at a different *k* value than its conduction band maximum (red line), again confirming an indirect gap in spite of the order of magnitude higher potential employed.
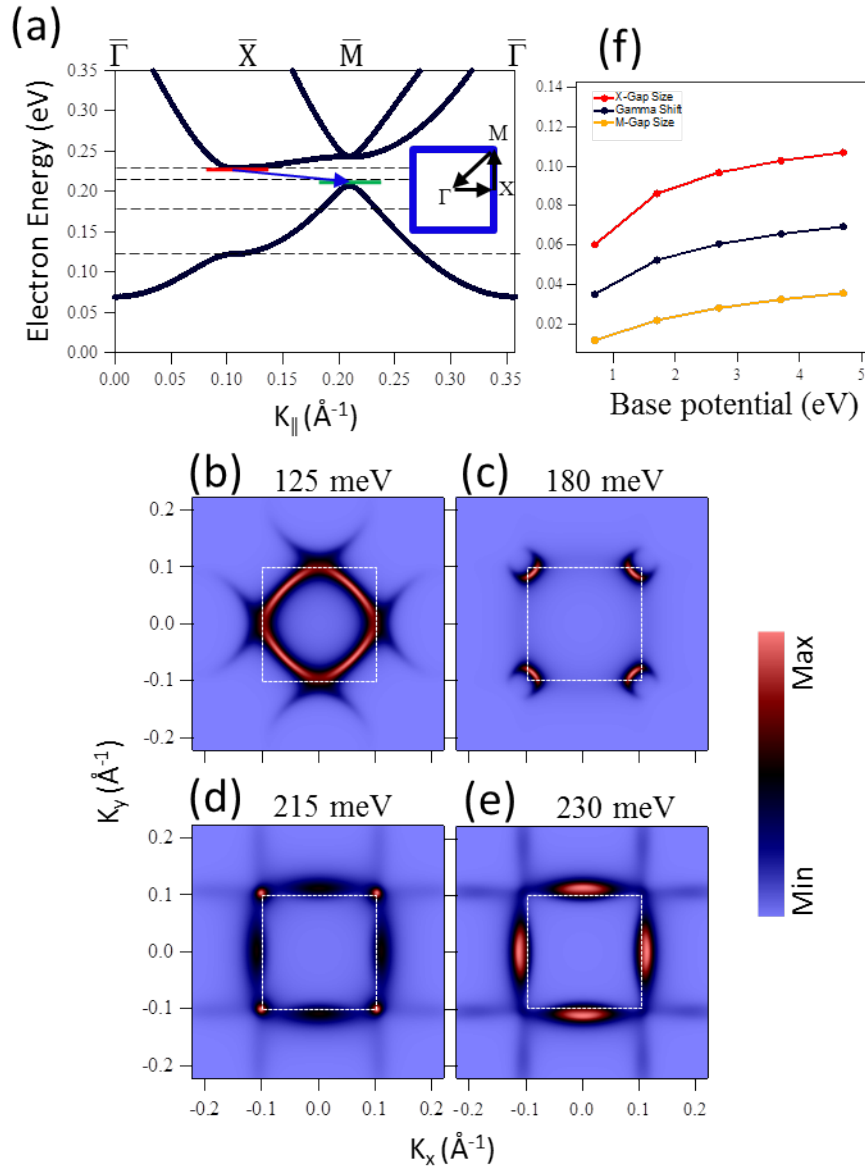
Figure 4: a. Calculated band structure using EPWE along the $\overline{\Gamma X M \Gamma}$ direction for a square patterned metal surface with circular bases potential of 4.7 eV and lattice parameter *d* = 3 nm. (b-e) The simulated constant energy surfaces using EPWE taken at the four electron energies. (f) The variation of $\overline{\Gamma}$-point shift (blue) and both $\overline{X}$-point (red) and $\overline{M}$-point (yellow) gaps size as a function of the circular base potential V_1.

Figures 4(b-e) present the simulated CESs taken at the black dashed lines in (a), i.e., at 125 meV, 180 meV, 215 meV, and 230 meV, respectively. The CES in (b) is taken at the lower edge of the $\overline{X}$-gap, and exhibits intensity reduction only at the four equivalent $\overline{X}$-points, confirming the beginning of energy gaps at these points. Right at the center of $\overline{X}$-gap, the intensity reduction was enhanced for all *k*-points on the surface BZ, except for the

corners defining the $\overline{M}$-points (c). At electron energy of the conduction band minimum, $E = 215$ meV, the hole pockets close into defined points, with the emergence of weak intensity due to the proximity of the bottom of the conduction (d). The last CES in (e) is taken approximately at the center of the $\overline{M}$-gap, i.e., the low intensity in the BZ corners is increased. By EPWE, five electronic band dispersions of squarely patterned metal surface were calculated to investigate the effect of periodic potential barrier V_1 on the semiconducting band gap size, and $\overline{\Gamma}$-point energy. The resulting $\overline{\Gamma}$-point energy (blue), $\overline{X}$-point gap size (red) and $\overline{M}$-point gap size (yellow) as a function of V_1 are presented in Fig. 4(f). It is clear that both the $\overline{\Gamma}$-point energy and $\overline{M}$-point gap size increase rapidly with the scattering potential, and tend to saturate at higher V_1 values. The highest potential where these saturate sets the infinite potential limit of the given system.

3.3. Effect of periodicity

The Bloch wave function has an exponential proportion with the reciprocal lattice vector G, i.e., inverse relationship between the effective periodic potential V and the superlattice constant d. This entails that the bigger the superlattice periodicity, the smaller the effect of periodic potential is. This is the motivation to discuss the effect of superlattice periodicity on surface state of the square superlattice presented here.

The simulated CESs of a squarely patterned metal surface with a potential barrier height V=700 meV and a superlattice constant $d = 5$ nm are presented in Fig. 5(a-d). To demonstrate the effect of the modified d, these CESs are taken at the edges of the corresponding surface state gaps, i.e., at 40 meV, 50 meV, 65 meV, and 75 meV, respectively. Actually one can determine the $\overline{X}$-point gap edges and size from the first CESs. Figure 5(a) confirms the beginning of $\overline{X}$-point energy gaps, the main and umklapp bands back-folding are satisfied at the four equivalents $\overline{X}$-points.

The intensity lowering was developed in (b) for all k-points on the surface BZ, except for the corners defining the $\overline{M}$-points, i.e., the CES taken at the center of $\overline{X}$-point energy gap. Clearly seen is the high intensity of allowed stats at the BZ boundaries demonstrating the lower edges of the four equivalents $\overline{X}$-gaps in (c). Based on this, the $\overline{X}$-point gap size is reduced from 60 meV in Fig. 2, to 25 meV for this surface state. Likewise, the $\overline{M}$-point gap size is reduced to 2 meV (d), and the $\overline{\Gamma}$-point energy become 10 meV. To discuss the three preceding dispersion parameters as a function of superlattice constant (expressed as $1/d$), five electronic band structures were calculated by EPWE, where the superlattice periodicity (d) is changed gradually from 3 nm and 5 nm. The three curves in Fig. 5(e) confirmed the behavior analogy between the periodicity reduction and potential barrier enhancement.

4. Constrains and limitations

During this study the atomic details are not taken into account. This is a valid approach only when treating the electronic surface states. For electronic states which have wavelength of the order of the atomic lattice, such as bulk states, the atomic structure is crucial for the proper description of the band structure. In this context, methods such as density functional theory (DFT) could be employed.
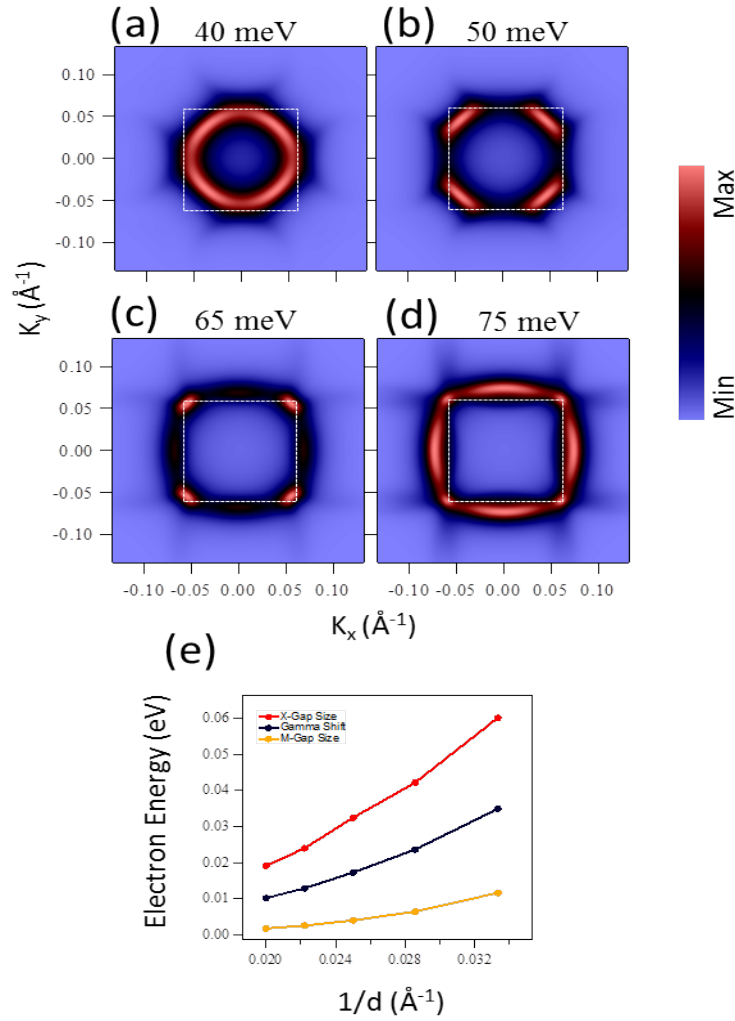
Figure 5: (a,b,c,d) Simulated Constant energy surfaces using EPWE for a square patterned metal surface of circular potential with 700 meV and lattice parameter d = 5 nm. The preceding CESs taken at the four electron energies, i.e. at 40, 50, 65, and 75 meV respectively. (e) Each of $\bar{\Gamma}$-point shift (blue), $\bar{X}$-gap size (red), and $\bar{M}$-gap size (yellow) as a function of the superlattice constant (expressed as 1/d).

5. Conclusion

It has been shown that the band structure of square metallic superlattices, with circular bases as scatterers, is characterized by an indirect semiconducting energy gap and the surface state exhibit a rigid upward energy shift. Evidence of this semiconducting gap is also seen in the LDOS, where 2D-maps of LDOS taken at energies around this gap were not identical. Furthermore, it has been possible to tune this energy gap size and the $\bar{\Gamma}$-point energy through both the barrier height and superlattice periodicity.

Acknowledgements

References

[1]. T. Greber and C. Oshima, J. Phys.: Condens. Matter, 2012, 24, 310201.

[2]. F. Schwierz, Nat. Nanotechnol., 2010, 5, 487–496.

[3]. J. D. Fowler, M. J. Allen, V. C. Tung, Y. Yang, R. B. Kaner and B. H. Weiller, ACS Nano, 2009, 3, 301–306.

[4]. H. Ma, T. Brugger, S. Berner, Y. Ding, M. Iannuzzi, J. Hutter, J. Osterwalder and T. Greber, ChemPhysChem, 2010, 11, 399–403.

[5]. B. Wang and M.-l. Bocquet, J. Phys. Chem. Lett., 2011, 2, 2341–2345.

[6]. ludwig bartels, "review article: tailoring molecular layers at metal surfaces", nature chemistry, VOL 2, FEBRUARY 2010.

[7]. Cicoira, F.; Rosei, F. Surf. Sci. 2006, 600, 1.

[8]. Aı̈t-Mansour, K.; Ruffieux, P.; Xiao, W.; Gro¨ning, P.; Fasel, R.; Gro¨ning, O. Phys. ReV. B: Condens. Matter Mater. Phys. 2006, 74, 195418.

[9]. Xiao, W.; Ruffieux, P.; Aı̈t-Mansour, K.; Gro¨ning, O.; Palotas, K.; Hofer, W. A.; Gro¨ning, P.; Fasel, R. J. Phys. Chem. B 2006, 110, 21394.

[10]. Matsumoto, Y.; Tanaka, K. Jpn. J. Appl. Phys. 1998, 37, 154.

[11]. Komori, F.; Ohno, S.; Nakatsuji, K. Prog. Surf. Sci. 2004, 77, 1.

[12]. Rosei, F.; Schunack, M.; Naitoh, Y.; Jiang, P.; Gourdon, A.; Laegsgaard, E.; Stensgaard, I.; Joachim, C.; Besenbacher, F. Prog. Surf. Sci. 2003, 71, 95.

[13]. S. LaShell, B. A. McDougall, and E. Jensen, Phys. Rev. Lett. 77(16), 3419 (1996).

[14]. P. O. Gartland and B. J. Slagsvold, Phys. Rev. B 12(10), 4047 (1975).

[15]. Zakaria Abd El-Fattah, Ph.D Thesis, Surface states manipulation via surface/interface defects and adsorbates, September 2012, and references therein.

[16]. F Schiller, Z M Abd El-Fattah, S Schirone, J Lobo-Checa, M Urdanpilleta, M Ruiz-Osés, J Cordón, M Corso1, D Sánchez-Portal, A Mugarza and J E Ortega, New J. Phys. 16 (2014) 123025.

[17]. A. Bendounan, F. Forster, J. Ziroff, F. Schmitt, and F. Reinert, PHYSICAL REVIEW B 72, 075407 2005.

[18]. J. Lobo-Checa, M. Matena, K. Müller, J. H. Dil, F. Meier, L. H. Gade, T. A. Jung, and M. Stöhr, Science 325, 300 (2009).

[19]. Bin Lu, Takushi Iimori, Kazuyuki Sakamoto, Kan Nakatsuji, Federico Rosei, and Fumio Komori, J. Phys. Chem. C, Vol. 112, No. 27, 2008.

[20]. Mervyn Roy, The central equation, May 6, 2015.

[21]. F. Reinert, G. Nicolay, S. Schmidt, D. Ehm, and S. Hüfner, Phys. Rev. B 63, 115415 (2001).

[22]. K. Oura, V. G. Lifshits, A. A. Saranin, A. V. Zotov, and M. Katayama, Surface Science: An Introduction, Berlin: Springer-Verlag, 2003.

[23]. G. Vasseur, Y. Fagot-Revurat, B. Kierren, M. Sicot, and D. Malterre, Symmetry 5, 344 (2013).